IEEE Access
Multidisciplinary | Rapid Review | Open Access Journal

Received 15 June 2022, accepted 24 June 2022, date of publication 29 June 2022, date of current version 5 July 2022.

Digital Object Identifier 10.1109/ACCESS.2022.3187031

RESEARCH ARTICLE

Fault-Tolerant Control of Automated Guided Vehicle Under Centroid Variation

QINGJIE ZHANG, WEI LIU, AND PING LIU
School of Automotive Engineering, Yancheng Institute of Technology, Yancheng, Jiangsu 224051, China

Corresponding author: Wei Liu (liuwei@ycit.edu.cn)

This work was supported in part by the National Natural Science Foundation of China under Grant 51405419, in part by the Natural Science Foundation of the Jiangsu Higher Education Institutions of China under Grant 18KJB460029, in part by the Postgraduate Research & Practice Innovation Program of Yancheng Institute of Technology under Grant SJCX21_XZ00 and Grant SJCX21_XY021, and in part by the Excellent Master Thesis Cultivation Project of Yancheng Institute of Technology under Grant LWPY2208.

ABSTRACT Aiming at stability and safety problems caused by the actuator failure of the automated guided vehicle under the condition of centroid position change. The four-wheel independent drive four-wheel independent steer (4WID/4WIS) AGV is studied for fault-tolerant control of single-wheel drive actuators under the centroid position variation condition. First, 3-DOF vehicle model, drive-wheel dynamics model, HSRI tire model, and the actuator loss of effectiveness model established. Second, a hierarchical controller is designed with an optimal input controller based on Model Predictive Control (MPC) theory of the upper layer, a desired yaw moment solver based on fuzzy theory of the middle layer, and a torque reconstruction controls distributor based on the control gain in the lower layer. Then, the AGV is simulated and analyzed in straight line and double line change conditions. The simulation results show that the yaw rate and the centroid sideslip angle can closely track the theoretical value. The difference between the theoretical value is kept within 5%. Finally, the 4WID/4WIS AGV prototype vehicle was developed and tested for straight-line and double-lane change condition. The difference between simulation and experiment was within 4%. The experimental results show that the designed controller is effective.

INDEX TERMS 4WID/4WIS, MPC, fault-tolerant control, drive torque reconstruction, centroid variation.

I. INTRODUCTION

The 4WID/4WIS AGV is a typical over-drive control system with drive chain short, structure compact and high degree of control freedom. In recent years, the application of active safety technologies such as traction control system (TCS), steer- by-wire (SBW), direct yaw rate moment control (DYC) and 6G communication networks [1] has increased the complexity of the system and the number of control actuators while improving driving safety and flexibility. For the most part, the AGV works in a harsh environment, increasing the probability of driving system failure and creating the problem of handling tasks not total between stations, which places higher demands on the real-time and reliability of fault-tolerant control.

Domestic and foreign scholars have conducted research on fault-tolerant control (FTC) of drive actuators based on making full use of the over-redundancy characteristics of 4WID/4WIS vehicles [2]–[4]. FTC is generally divided into two categories, namely passive fault-tolerant control (PFTC) and active fault-tolerant control (AFTC). PFTC is a feedback control that enables closed-loop control. Robust to specific faults and does not require fault details exactly are easy to implement. Feedback linearization method (FLM) has found many applications in solving nonlinear system problems. Cooperative game theory is introduced in the FLM framework by considering the four drive actuators as participants and deriving pareto strategies among the participants based on distributed model predictive control (DMPC) using convex iterative method [5]. It can also be combined with terminal sliding membrane control (TSMC) for complementary advantages to produce higher robustness [6]. Nevertheless, FLM cannot handle unexpected disturbances generated externally, modeling uncertainties, and coupling effects between drivers [7]. Sliding mode control (SMC) has received an army of attention from researchers in the

The associate editor coordinating the review of this manuscript and approving it for publication was Shaohua Wan.

field of FTC due to its insensitivity and robustness to perturbations and uncertainties. Common control strategies include the torque quadratic programming based on the use of an adaptive variable exponential convergence rate [8] or the exact reconfiguration of the actuator torque using the sliding mode variably structure equivalence principle based on the estimate of fault states, disturbances and the control gain of fault using an observer [9]–[11]. The grouping of drive actuators in the SMC framework is innovative. Each group of actuators implements a specific control objective, rearranging the steering geometry according to the wheel position of fault, and effectively avoids strong coupling effects between the control objectives [12]. The combination of predictive control and reconfiguration control methods allows for the vehicle post-failure stability control [13], and reconfiguration of the drive-wheel control force can alleviate the failed wheel torque demand [14]. The implementation of multi-method toggle FTC enables torque reconfiguration based on real-time operating conditions to improve power performance while ensuring stability [15], [16]. Similar to multi-method switching FTC there is also multi-model switching FTC, which enables stable exchange of dynamic data, identification of the match between the current operating state and the set of typical operating modes, and smooth switching of the control method according to the real-time state [17]. It is worth noting that it is impractical to consider the vehicle longitudinal speed as a constant in the controller design [18]. Considering the problem that the vehicle longitudinal velocity is time-varying and the uncertainty of actuator saturation due to the failure of the drive actuator, a non-fragile linear parameter-varying (LPV) that satisfies the vehicle dynamics is proposed to limit the centroid sideslip angle and the yaw rate to ensure the lateral stability and handling performance of the vehicle [19].

The above researches are all PFTC, where the controller is designed offline without changing the structure and parameters, which may lead to closed-loop systems that are insensitive to certain types of faults. AFTC is a future-oriented feed-forward control with higher adaptiveness to the time and magnitude of faults than PFTC, which can improve the performance of the control system to a greater extent. Difference from previous studies is focusing on fault detection and isolation (FDI) [20], [21]. In response to the current distributed drive vehicle FTC over-reliance on accurate vehicle dynamics model and fault diagnosis and detection (FDD), a multi-input multiple output no model adaptive fault-tolerant control method is proposed to collaborative drive the system to generate additional transverse swing moments to adaptively compensate for the faulty drive actuators [22]–[26] and achieve multi-objective optimization [27], [28]. Considering the effect of the difference between the torque demand and the actual torque input generated by inaccurate FDD in FTC on the stability of closed-loop control, the control assignment (CA) strategy and TSC is designed to be integrated to improve the robustness and stability under fault conditions [29]. Online optimization based on CA can effectively reduce the workload and computation time for fault-tolerant control of redundant systems [30]. The combination of ex ante control and ex post control allows for optimal performance of the vehicle after a failure. A control strategy combining baseline controller, reconfigurable controller and FDD is proposed to reconfigure the drive assignment based on real-time faults [31], [32]. Finite-time FTC is important for practical systems, namely, to eliminate the effects of drive actuator failures and nonlinear disturbance inputs in finite time so that the control input is limited to the desired constraint [33]. Shortening the recognition speed of FTC algorithm to achieve control in finite time is a common class of research directions such as the Kalman filter [34], the Unscented Kalman filter (UKF) [35], and the wavelet filter [36]. The discrete-time synthesis algorithm has the advantages of operation time fast, occupation space small and robustness, and is gradually used in finite-time FTC. Delta operator has the advantage of high sensitivity and fast sampling in the development of discrete-time integrated algorithms, combined with the fault tolerance of MPC [37]–[41] to preserve the steering capability while ensuring stability [42]. A coupled nonlinear dynamics discrete-time adaptive three-step control is proposed considering the vehicle tire adhesion limit characteristics. The algorithm achieves coordinated lateral and longitudinal control by adaptively updating the law and controller reconfiguration in discrete time [43]. The subjects of the above research are all passenger cars, and the effect of the change of the centroid position on the drive actuator FTC is negligible. Nevertheless, when the object of research is changed to an AGV, the load size random and position casual in the course of operation will lead to changes in the centroid position. This will cause the system's input and output unbounded, eccentric moment generation to the motion performance overall of the AGV to interfere with the problem is not considered in the former scholars.

Thus, the main contributions and innovations of this paper are as follows:

1) When considering yaw stability control for passenger cars, the centroid is simplified to a parametric constant for the vehicle. However, AGV changed the position of the vehicle's centroid in the course of operation due to changes in load size and position. Few dynamics control strategies have investigated effect of changes in the centroid position on dynamics. Therefore, the research of control strategies for centroid variation conditions is innovative.

2) The research of the drive actuator FTC while considering changes in the position of the centroid is place higher demands of accuracy requirements and real-time on the controller. This paper takes a highly redundant 4WID/4WIS system as an entry point for the synergistic cooperation of multiple actuators and the precise reconfiguration of drive torque distribution based on fault information specific to improve safety and stability.

3) A single control method cannot meet the current needs of multi-objective optimisation. In this paper, the MPC is used as the main controller of the system to exploit the

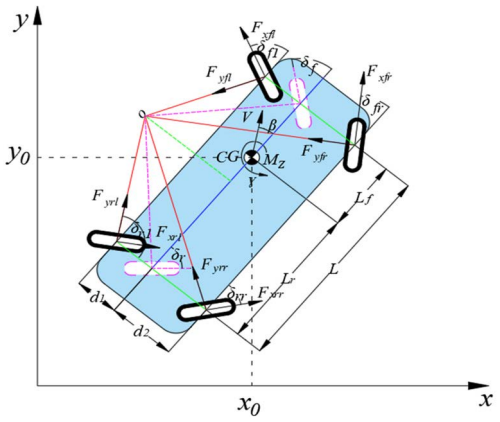

FIGURE 1. Vehicle dynamics model.

ability of rolling optimisation to find the optimal solution. Combined with fuzzy control, it makes full use of actuator state information to improve the performance and stability of the closed-loop system.

The rest of this paper organized is as follows. Chapter II establishes the model of the AGV system and problem statement; Chapter III designs the active fault-tolerant controller based on the centroid variable condition; Chapter IV simulates and analyzes the controller established; Chapter V conducting the algorithm verification experiments, and finally gives the conclusion in Chapter VI.

II. SYSTEM MODEL AND PROBLEM STATEMENT

A. VEHICLE DYNAMICS MODEL

This paper takes the AGV as the research object and the whole vehicle adopts wire control technology. Four hub motors and four steering motors are used as drive actuators. In the design of the over-redundant mechanism control system, a simplified model that can reflect the basic characteristics of the vehicle system is required, as shown in FIGURE 1.

In FIGURE 1, CG is the AGV centroid, x_o is the component of the centroid on the x-axis of the absolute coordinate system, y_o is the component of the centroid on the y-axis of the absolute coordinate system, and V is the vehicle's centroid velocity. Where including longitudinal, lateral and lateral motion, the motion equation is as follows:

Longitudinal motion equation:

$$\begin{aligned} m\left(\dot{v}_x - v_y\gamma\right) = {} & F_{xfl}\cos\delta_{fl} + F_{xfr}\cos\delta_{fr} + F_{xrl}\cos\delta_{rl} \\ & + F_{xrr}\cos\delta_{rr} + F_{yrl}\sin\delta_{rl} + F_{yrr}\sin\delta_{rr} \\ & - F_{yfl}\sin\delta_{fl} - F_{yfr}\sin\delta_{fr} \end{aligned} \tag{1}$$

In the motion equation, m is the AGV quality, $\dot{v}_x$ is the longitudinal acceleration, v_y is the lateral velocity of the centroid in the vehicle body coordinate system, γ is the yaw rate, and F_{xi} and F_{yi} $(i = fl, fr, rl, rr)$ are the tire longitudinal force and lateral force. δ_{fl} and δ_{fr} are the left and right steering angles of the front wheels, δ_{rl} and δ_{rr} are the left and right steering angles of the rear wheels.

Lateral motion equation:

$$\begin{aligned} m\left(\dot{v}_y + v_x\gamma\right) = {} & F_{xfl}\sin\delta_{fl} + F_{yfl}\cos\delta_{fl} + F_{xfr}\sin\delta_{fr} \\ & + F_{yfr}\cos\delta_{fr} + F_{yrl}\cos\delta_{rl} + F_{yrr}\cos\delta_{rr} \\ & - F_{xrl}\sin\delta_{rl} - F_{xrr}\sin\delta_{rr} \end{aligned} \tag{2}$$

In the motion equation, $\dot{v}_y$ is the lateral acceleration, v_x is the longitudinal velocity of the centroid in the vehicle body coordinate system.

Yaw motion equation:

$$\begin{aligned} I_z\dot{\gamma} = {} & L_f\begin{pmatrix} F_{xfl}\sin\delta_{fl} + F_{yfl}\cos\delta_{fl} \\ +F_{xfr}\sin\delta_{fr} + F_{yfr}\sin\delta_{fr} \end{pmatrix} \\ & + L_r\begin{pmatrix} F_{xrl}\sin\delta_{rl} - F_{yrl}\cos\delta_{rl} \\ +F_{xrr}\sin\delta_{rr} + F_{yrr}\cos\delta_{rr} \end{pmatrix} \\ & + d_1\begin{pmatrix} F_{yfl}\sin\delta_{fl} - F_{xfl}\cos\delta_{fl} \\ -F_{yrl}\sin\delta_{rl} - F_{xrl}\cos\delta_{rl} \end{pmatrix} \\ & + d_2\begin{pmatrix} F_{xfr}\cos\delta_{fr} - F_{yfr}\sin\delta_{fr} \\ +F_{xrr}\cos\delta_{rr} + F_{yrr}\sin\delta_{rr} \end{pmatrix} \end{aligned} \tag{3}$$

In the motion equation, I_z is the inertia moment of the AGV around the z-axis, γ is the yaw angular acceleration, L_f and L_r are the distances from the centroid to the front and rear axles respectively, d_1 and d_2 are the distance from left and right wheels to the equivalent wheels respectively.

Take one driving wheel as an example, considering the dynamic characteristics of wheels, and ignoring friction and rolling resistance. The differential equation of wheel motion can be written as:

$$J_\omega\dot{\omega}_i = T_i - F_{xi}R \tag{4}$$

In the equation, J_ω is the wheel inertia moment, $\dot{\omega}_i$ is the wheel rotation angular acceleration, T_i is the wheel input torque, R is the wheel effective rolling radius, $i = (fl, fr, rl, rr)$.

Considering that the actual longitudinal force and lateral force of the tire difficult to measure, but the design of the controller requires calculation fast and accurate. In this paper, the HSRI (Highway Safety Research Institute) tire model is established to estimate the lateral force and longitudinal force of the tire.

$$\begin{cases} F_{xi} = \begin{cases} C_x\lambda_i/(1-\lambda_i), & H < 1/2 \\ (C_x\lambda_i/(1-\lambda_i))\left(1/H - 1/\left(4H^2\right)\right), & H \geq 1/2 \end{cases} \\ F_{yi} = \begin{cases} C_y\tan\alpha_i/(1-\lambda_i), & H < 1/2 \\ \left(C_y\tan\alpha_i/(1-\lambda_i)\right)\left(1/H - 1/\left(4H^2\right)\right), & H \geq 1/2 \end{cases} \end{cases} \tag{5}$$

where

$$H = \sqrt{\left(\frac{\lambda_i}{1-\lambda_i}\bullet\frac{C_x}{\mu F_{zi}}\right)^2 + \left(\frac{1}{1-\lambda_i}\bullet\frac{C_x}{\mu F_{zi}}\tan\alpha\right)^2}$$

In the equation, C_x and C_y are tire longitudinal stiffness and cornering stiffness respectively, α_i, λ_i are tire cornering

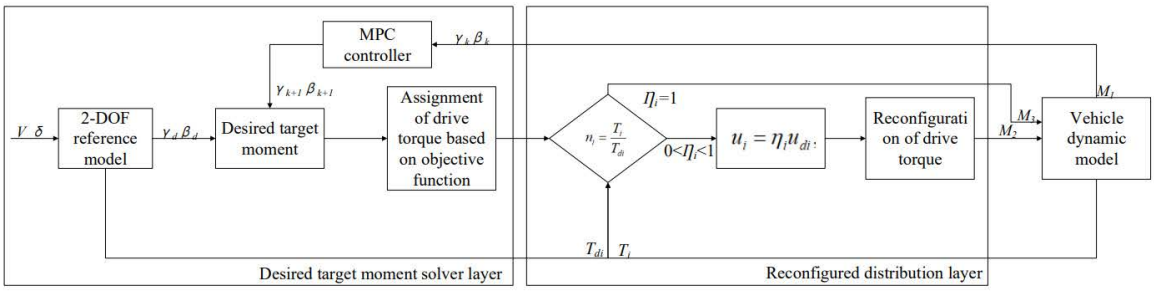

FIGURE 2. System control block diagram.

TABLE 1. Drive actuator failure fault parameters.

Fault types	Value of η_i	Value of ΔT_i
Loss of effectiveness	$0<\eta_i<1$	$\Delta T_i=0$
Healthy	$\eta_i=1$	$\Delta T_i=0$

angle and slip rate respectively, F_{zi} is the vertical force of each wheel tire, and μ_i is the road adhesion coefficient.

Remark 1: Estimation of the vertical force F_{zi} for each wheel by means of a triaxial accelerometer [44] embedded in the tyre.

B. ACTUATOR FAILURE MODEL

The research goal of this paper is to realize the yaw stability control when a single drive actuator fails under the centroid variation condition. The failure state can be expressed in a unified form:

$$T_i = \eta_i T_{di} + \Delta T_i \tag{6}$$

In the equation, T_i is the actual drive actuator expected control force, T_{di} is the expected output torque of each motor. ΔT_i is the additional torque caused by a faulty drive actuator, η_i is the control gain. When $\eta_i = 1$, $\Delta T_i = 0$, the drive actuator is in a healthy state; When $\eta_i = 1$, $\Delta T_i = c$, the drive actuator is in a additive fault state; When $\eta_i = 0$, $\Delta T_i = \mathrm{c}$, the drive actuator is in a stuck at fixed level fault state; When $\eta_i \in (0, 1)$, $\Delta T_i = 0$, the drive actuator is in a loss of effectiveness state, c is a constant. This paper only considers the loss of effectiveness state.

Remark 2: The solution of T_i can further calculate the driving force F, so as to obtain the inputs F_{xi} and F_{yi} in the dynamic model. This paper focuses on the loss of effectiveness of one of the drive actuators. Table 1 summarizes the relationship between actuator failure and η_i.

The research goal of this paper is to realize the dynamic reconstruction torque compensation for the drive actuator loss of effectiveness under the centroid variation condition. It is assumed that the fault information required has been obtained from the ideal FDD system, but any FDD algorithm will have certain errors. The error of models is between the actual fault E and the measurement fault E*, which can refer (7)

$$\|\Delta E\| = \left\|E - E^*\right\| \leq \lambda \tag{7}$$

Refer (7), $\lambda > 0$ indicates the degree of the FDD system inaccuracy within the known range in the controller design.

C. PROBLEM STATEMENT

This paper takes 4WID/4WIS AGV as the research object, and researches the yaw stability control for the problem of drive actuator loss of effectiveness under the condition of varying centroid.

Refer FIGURE 2, in order to solve the above problem, this paper uses AFTC based on layered control, which consists of MPC controller layer, expectation target torque layer and control gain-based torque reconstruction layer. When AGV is operating, the uneven load weight and the irregular placement will cause the centroid position to change. When the AGV is in the unstable state, the controller will input the target vehicle speed V and wheel rotation angle δ into the 2-DOF reference model to generate the expectation yaw rate γ_d and expectation centroid sideslip angle β_d. γ_d, β_d and the actual measured yaw rate γ and the centroid sideslip β of the AGV MPC controller is differenced to obtain $\Delta\gamma$, $\Delta\beta$. First, the desired yaw moment is solved by fuzzy theory, and the driving force is assigned according to the objective function. Next, the desired output torque obtained from the reference model is differenced the actual output torque measured by the actual sensor to obtain the control gain, and to determine whether there is a loss of effectiveness fault in the four drive actuators. Provided that $\eta_i = 1$, there is no fault and the drive torque is distributed according to the objective function. Provided that $0 < \eta_i < 1$, there is a loss of effectiveness fault. The fault needs to be modeled and the solved desired drive torque is input into the torque reconstruction module. According to different fault conditions, different reconfiguration control rates are used, and finally the reconfigured drive force is distributed to the drive actuators to achieve the stability of the AGV.

III. AFTC DESIGN

A. MPC CONTROLLER DESIGN

MPC is a non-linear feedback control strategy applied to predict the future state of the system based on the model

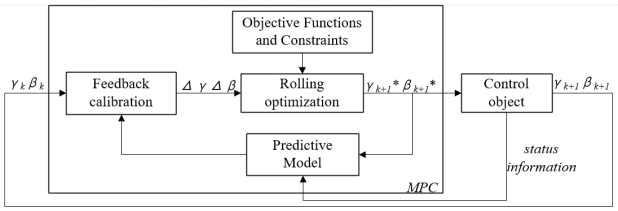

FIGURE 3. MPC control flow chart.

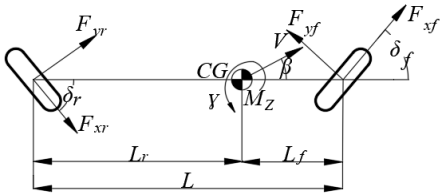

FIGURE 4. 2-DOF reference model.

established. The error between the predicted and actual output can be reduced by rolling optimization and the optimization problem is continuously refreshed to achieve optimal control in a locally finite time. The MPC control flow chart in this paper is shown in FIGURE 3.

Refer FIGURE 3, when the centroid position changes or the drive actuator fails during AGV operation leading to instability, MPC solves the γ_k^*, β_k^* of the controlled object at the moment k by the prediction model, and the γ_k, β_k of the real-time state of the controlled object estimated by the sensor is processed as a difference for feedback correction. The obtained $\Delta\gamma$, $\Delta\beta$ is rolled and optimized based on the objective function and constraints to obtain γ_{k+1}^*, β_{k+1}^* at k+1 moments, and acting on the controlled to turn thumbs down on realize the closed-loop control and solve for the optimal solution in finite time.

The accuracy of the prediction model determines the control effect of the MPC controller, but as the accuracy increases, the mathematical model becomes more complex and the computational volume rises, leading to a decrease in real-time making the control system useless. Considering that MPC itself has the characteristics of feedback correction and has certain robustness. Therefore, the prediction model in this paper chooses a 2-DOF reference model as shown in FIGURE 4, which can be expressed by the equation:

$$\begin{cases} mv\left(\dot{\beta}+\gamma\right) = k_f\left(\beta+\dfrac{L_f\gamma}{v}-\delta_f\right)+k_r\left(\beta-\dfrac{L_r\gamma}{v}-\delta_r\right) \\ I_z\dot{\gamma} = k_fL_f\left(\beta+\dfrac{L_f\gamma}{v}-\delta_f\right)-k_rL_r\left(\beta-\dfrac{L_r\gamma}{v}-\delta_r\right) \end{cases} \tag{8}$$

where δ_f, δ_r is the front wheel steering angle and rear wheel steering angle of the 2-DOF reference model respectively, and k_f, k_r is the front wheel lateral deflection stiffness and rear wheel lateral deflection stiffness of the 2-DOF reference model respectively.

Express equation (8) as a state-space expression of the system in the following form:

$$\begin{cases} \dot{x}(t) = A_cx(t)+B_cu(t) \\ y_c(t) = C_cx(t) \end{cases} \tag{9}$$

where

$$A_c = \begin{bmatrix} \dfrac{k_f+k_r}{mv} & \dfrac{k_fL_f-k_rL_r}{mv^2}-1 \\ \dfrac{k_fL_f-k_rL_r}{I_z} & \dfrac{k_fL_f^2+k_rL_r^2}{I_zv} \end{bmatrix},$$

$$B_c = \begin{bmatrix} -\dfrac{k_f}{mv} & -\dfrac{k_r}{mv} \\ -\dfrac{k_fL_f}{I_z} & \dfrac{k_rL_r}{I_z} \end{bmatrix}, \quad C_c = \begin{bmatrix} 1 & 0 \\ 0 & 1 \end{bmatrix},$$

$$x(t) = \begin{bmatrix} \beta \\ \gamma \end{bmatrix} \quad u(t) = \begin{bmatrix} \delta_f \\ \delta_r \end{bmatrix}$$

Discretizing equation (9):

$$\begin{cases} x(k+1) = Ax(k)+Bu(k) \\ y_c(k) = C_cx(k) \end{cases} \tag{10}$$

To satisfy the MPC solution requirements, equation (11) is rewritten in incremental form:

$$\begin{cases} \Delta x(k+1) = A\Delta x(k)+B\Delta u(k) \\ y_c(k) = C_c\Delta x(k)+y_c(k-1) \end{cases} \tag{11}$$

where, $A=e^{AcTs}$, $B=\int_0^{Ts}e^{A_c\tau}d\tau \bullet B_c$,

$\Delta x(k) = x(k)-x(k-1)$, $\quad \Delta u(k) = u(k)-u(k-1)$.

Based on the current AGV state information x(k), y(k), the state variable values in the future p sampled time domains can be predicted, namely:

$$\begin{aligned} &\Delta x(k+p\,|k) \\ &\quad = A\Delta x(k+p-1\,|k)+B\Delta u(k+p-1) \\ &\quad = A^pA\Delta x(k)+A^{p-1}B\Delta u(k)+A^{p-2}B\Delta u(k+1) \\ &\qquad +\ldots\ldots+A^{p-m}B\Delta u(k+m-1) \end{aligned} \tag{12}$$

$$\begin{aligned} &Y_p(k+1\,|k) \\ &\quad = S_x\Delta x(k)+\Gamma y_c(k)+S_u\Delta U(k) \end{aligned} \tag{13}$$

where, $Y_p(k+1\,|k)$ and S_u, as shown at the bottom of the next page.

MPC online finite time domain rolling optimization module needs to be carried out based on certain objective function, this paper researches the instability caused by the change of centroid position or drive actuator loss of effectiveness of the AGV, so the stability function is used for optimization, namely:

$$J_{stb} = \left\|\tau_y\left(Y_p(k+1\,|k)-R(k+1)\right)\right\|^2+\|\tau_u\Delta U(k)\|^2 \tag{14}$$

where, τ_y is a matrix of weighting coefficients related to vehicle state deviations, τ_u is a matrix of weighting

coefficients related to the rate of change of control quantities. The first term in the equation indicates that the AGV output follows the desired output, and the second term indicates that the amount of control should not be too large and thus affect the AGV stability.

To ensure optimal control performance after AGV destabilization, the following constraints on the inputs need to be applied according to the actual conditions:

$$\begin{cases} u_{\min}(k+i) \le u(k+i) \le u_{\max}(k+i), \\ \quad i = 0, 1, \cdots, m-1 \\ \Delta u_{\min}(k+i) \le \Delta u(k+i) \le \Delta u_{\max}(k+i), \\ \quad i = 0, 1, \cdots, m-1 \\ x_{\min}(k+i) \le x(k+i) \le x_{\max}(k+i), \\ \quad i = 0, 1, \cdots, p \\ \dot{x}_{\min}(k+i) \le \dot{x}(k+i) \le \dot{x}_{\max}(k+i), \\ \quad i = 0, 1, \cdots, p \end{cases} \tag{15}$$

B. EXPECTATION TARGET MOMENT LAYER

The expectation target moment layer contains two modules: the desired yaw moment and the target function-based drive force assignment. When the AGV is in the centroid variation condition, this paper adopts a controller based on fuzzy theory, which takes $\Delta\gamma$, $\Delta\beta$ as input quantities and solves the output quantity expected transverse swing moment M_d after fuzzification, fuzzy inference and defuzzification. The fuzzy controller input and output affiliation functions are chosen as triangular functions. According to the system model, the input and output theoretical domains is [−1 1], the input fuzzy sets are [NB, NS, ZO, PS, PB], and the output fuzzy sets are [NB, NM, NS, ZO, PS, PM, PB]. With $\Delta\gamma$ and $\Delta\beta$ as the control parameters, the "Mamdani" type reasoning and the area center of gravity method used for defuzzification, and M_d is finally solved.

The M_d solved by the fuzzy controller needs to satisfy the yaw moment generated by each drive actuator and ground force on the AGV centroid. Therefore, the target torque assigned to each drive actuator needs to satisfy the following constraints:

$$\begin{cases} T_{fr} + T_{fl} + T_{rr} + T_{rl} \\ \quad = T_d \left(T_{fr}\cos\delta_{fr} + T_{rr}\cos\delta_{rr}\right) d_2 \\ \quad\quad - \left(T_{fl}\cos\delta_{fl} + T_{rl}\cos\delta_{rl}\right) d_1 \\ \quad\quad + \left(T_{fr}\sin\delta_{fr} + T_{fl}\sin\delta_{fl}\right) L_f \\ \quad\quad + \left(T_{rl}\sin\delta_{rl} - T_{rr}\sin\delta_{rr}\right) L_r = M_d R \end{cases} \tag{16}$$

where T_i is the drive actuator torque and T_d is the total AGV drive torque.

When AGV advances, motor torque output must also meet the requirements of the actual application. Namely, no negative torque, no more than the maximum output torque and consider the constraints of the road conditions. Therefore, the following constraints need satisfy:

$$\begin{cases} 0 \le T_i \le D_i T_{i\max} \\ \dfrac{T_i}{R} \le \mu_i F_{zi} \end{cases} \tag{17}$$

where T_{imax} is the maximum output torque of the drive.

For the destabilization problem caused by the change of the centroid position of AGV under the fault-free condition. This paper adopts the nominal control distribution rate with the objective of maximizing the tire adhesion margin and improving the vehicle stability. The objective function is as

$$Y_p(k+1|k) = \begin{bmatrix} y_c(k+1|k) \\ y_c(k+2|k) \\ \vdots \\ y_c(k+p|k) \end{bmatrix}_{p\times 1}, \quad \Delta U(k) = \begin{bmatrix} \Delta u(k) \\ \Delta u(k+1) \\ \vdots \\ \Delta u(k+m-1) \end{bmatrix}_{m\times 1}, \quad S_x = \begin{bmatrix} C_c A \\ \sum_{i=1}^{2} C_c A^i \\ \vdots \\ \sum_{i=1}^{p} C_c A^i \end{bmatrix}_{p\times 1},$$

$$S_u = \begin{bmatrix} C_c B & 0 & 0 & \cdots & 0 \\ \sum_{i=1}^{2} C_c A^{i-1} B & C_c B & 0 & \cdots & 0 \\ \vdots & \vdots & \vdots & \ddots & \vdots \\ \sum_{i=1}^{m} C_c A^{i-1} B & \sum_{i=1}^{m-1} C_c A^{i-1} B & \cdots & \cdots & C_c B \\ \vdots & \vdots & \vdots & \ddots & \vdots \\ \sum_{i=1}^{p} C_c A^{i-1} B & \sum_{i=1}^{p-1} C_c A^{i-1} B & \cdots & \cdots & \sum_{i=1}^{p-m+1} C_c A^{i-1} B \end{bmatrix}_{p\times m}, \quad \Gamma = \begin{bmatrix} I_{nc\times nc} \\ I_{nc\times nc} \\ \vdots \\ I_{nc\times nc} \end{bmatrix}_{p\times 1}$$

follows:

$$\min\ J = c_1\frac{F_{xfl}^2+F_{yfl}^2}{\mu_{fl}^2F_{zfl}^2}+c_2\frac{F_{xfr}^2+F_{yfr}^2}{\mu_{fr}^2F_{zfr}^2}+c_3\frac{F_{xrl}^2+F_{yrl}^2}{\mu_{rl}^2F_{zrl}^2}+c_4\frac{F_{xrr}^2+F_{yrr}^2}{\mu_{rr}^2F_{zrr}^2} \tag{18}$$

where c_1, c_2, c_3, c_4 are the weighting coefficients.

In the HSRI tire model, the following relationship exists between the lateral and longitudinal tire forces:

$$F_{yi} \approx \frac{C_y\alpha_i}{C_x\lambda_i}F_{xi} \tag{19}$$

Equation (18) can be written as:

$$\begin{aligned}\min\ J &= \sum_{i=4}^{4} c_i\frac{F_{xi}^2+F_{yi}^2}{(\mu_iF_{zi})^2}\\ &= \sum_{i=4}^{4} c_i\frac{F_{xi}^2}{(\mu_iF_{zi})^2}\left[1+\left(\frac{C_y\alpha_i}{C_x\lambda_i}\right)^2\right]\\ &= \sum_{i=4}^{4} c_i\frac{k_iF_{xi}^2}{(\mu_iF_{zi})^2}\end{aligned} \tag{20}$$

where,

$$k_i = 1+\left(\frac{C_y\alpha_i}{C_x\lambda_i}\right)^2$$

The (20) can be further simplified as:

$$\min\ J = x^TQx \tag{21}$$

where,

$$x = \begin{bmatrix}F_{xfl} & F_{xfr} & F_{xrl} & F_{xrr}\end{bmatrix}^T,\quad Q = diag\left(\frac{1}{\left(\frac{\mu_iF_{zi}}{c_i\sqrt{k_i}}\right)^2}\right)$$

In this paper, the quadratic programming method is used to solve the objective function, definite:

$$q = \begin{bmatrix}T_d & M_{zd}\end{bmatrix}^T,\quad p = \begin{bmatrix}T_{fl} & T_{fr} & T_{rl} & T_{rr}\end{bmatrix}^T = Rx$$

Then the equation constraint can be written as:

$$q = Bp \tag{22}$$

where B, as shown at the bottom of the page.

The above equations are modeled using Simulink with the input quantities $M_d, T_d, F_{zi}, v, \delta_{fl}, \delta_{fr}$. The quadratic programming algorithm of the embedded toolbox can be invoked to solve the objective function for the required stability under variable centroid conditions.

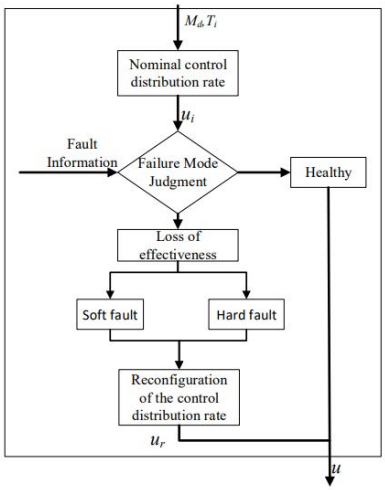

FIGURE 5. Torque reconstruction control flow chart.

C. MOMENT RECONFIGURATION LAYER

The instability caused by the centroid position variation of the AGV in the handling task between workstations in the smart factory can be controlled by the above stability-based nominal control distribution rate to complete the transverse pendulum stability control. However, when the drive actuator fails to provide the desired torque, the AGV can easily turn unstable again. Therefore, this paper investigates the loss of effectiveness of a single drive actuator, and when a single drive actuator fails, the output torque of three normal drive actuators is reconstructed according to the specific loss of effectiveness situation to generate additional transverse moment to improve the transverse stability of the vehicle while satisfying the longitudinal force requirement. The torque reconstruction control flow chart is shown in Fig.5.

In FIGURE 5, it can be seen that the reconfiguration control allocation method proposed in this paper is as follows:

The AGV travels under the change of centroid position and the control input u_i of each actuator is calculated using the nominal control distribution rate.

Based on the fault information, determine the form of failure of the drive actuator: Healthy, soft fault, hard fault.

Depending on the specific form of failure, the corresponding reconfiguration control distribution rate is used. At present, the actuator control input u is the reconfiguration actuator control input u_r.

1) CONTROL GAIN MODULE DESIGN

The relationship between the output torque of the drive actuator and the output power and speed is as follows:

$$T_i = 9550\frac{P_i}{n_i} \tag{23}$$

where P_i is the motor output power, n_i is the motor speed.

$$B = \frac{1}{R}\begin{bmatrix}1 & 1 & 1 & 1\\ L_f\sin\delta_{fl}-d_1\cos\delta_{fl} & L_f\sin\delta_{fr}+d_2\cos\delta_{fr} & L_r\sin\delta_{rl}-d_1\cos\delta_{rl} & -L_r\sin\delta_{rr}+d_2\cos\delta_{rr}\end{bmatrix}$$

Refer (23), it is known that when AGV travels at a certain speed and a certain drive actuator fails. It is necessary to ensure that the speed of the failed drive actuator remains unchanged if it wants to maintain the driving state currently, then the reduction of output power leads to the reduction of output torque. By bringing the calculation result of (23) into (6) and solving for the value of control gain η_i, it is possible to visualize the faulty drive actuator and its degree of loss of effectiveness, so that the desired drive torque can be reconstructed according to the failure situation specific to realize the yaw stability control after the change of centroid position and the loss of effectiveness of a single drive actuator.

2) TORQUE RECONFIGURATION MODULE DESIGN

For the 4WID/4WIS AGV, there are four cases according to the location of the faulty drive actuator, and this paper takes the left front drive actuator loss of effectiveness as an example for drive reconfiguration redistribution. Assuming that the lost torque of the left front drive actuator is T, then substituting $T_{fnew} = T_{fl} - T$ into (16) gives:

$$\begin{cases} T_{fr} + \left(T_{fl} - T\right) + T_{rr} + T_{rl} \\ \quad = T_{dnew}\left(T_{fr}\cos\delta_{fr} + T_{rr}\cos\delta_{rr}\right)d_2 \\ \quad\quad - \left[\left(T_{fl} - T\right)\cos\delta_{fl} + T_{rl}\cos\delta_{rl}\right]d_1 \\ \quad\quad + \left[T_{fr}\sin\delta_{fr} + \left(T_{fl} - T\right)\sin\delta_{fl}\right]L_f \\ \quad\quad + \left(T_{rl}\sin\delta_{rl} - T_{rr}\sin\delta_{rr}\right)L_r = M_{dnew}R \end{cases} \tag{24}$$

In order to maintain the current state of travel of the AGV, it is necessary to meet:

$$\begin{cases} T_{dnew} = T_d \\ M_{dnew} = M_d \end{cases} \tag{25}$$

Refer (18), the lateral force lost by the left front drive actuator can be compensated by increasing the output torque of the right front wheel drive actuator, and the loss of longitudinal force can be compensated by adjusting the output torque of the remaining normal drive actuators, namely,

$$\begin{cases} T_{flnew} = T_{fl} - T \\ T_{frnew} = T_{fr} + T \\ T_{rlnew} = T_{rl} + T\cos\delta_{fl} \\ T_{rrnew} = T_{rr} + T\cos\delta_{fl} \end{cases} \tag{26}$$

Similarly, when other driving actuators fail individually. They can all be solved according to equation (26), and according to the different values of η_i taken. They can be divided into three cases: healthy state, soft failure and hard failure, and the drive torque reconstruction redistribution strategy is shown in TABLE 2.

TABLE 2. Driver torque reconfiguration redistribution strategy.

Drive actuator failure conditions	Fault Constraints	Reconfigure control strategy
Healthy	T_{fl}=T_{di}	Residual control variables: T_{fl},T_{fr},T_{rl},T_{rr} Control Objectives: equation (18) Binding Conditions: equation (16),(17)
single drive actuator soft failure	T_{fl}=$\eta_i T_{di}$	Residual control variables: T_{fl},T_{fr},T_{rl},T_{rr} Control Objectives: equation (26) Binding Conditions: equation (24),(25)
single drive actuator hard failure	T_{fl}=0	Residual control variables: T_{fr},T_{rl},T_{rr} Control Objectives: equation (26) Binding Conditions: equation (24),(25)

TABLE 3. "Zhiyan V1" vehicle parameters.

Parameters	Value
vehicle quality/kg	108
Wheel roll radius/m	0.10
Wheelbase/m	0.59
Distance from the centroid to the front axle L_f/m	0.32
Distance from the centroid to the rear axle L_r/m	0.37
Vehicle rotational inertia I_z/($kg.m^2$)	70
Front and rear axle distance L/m	0.69

IV. SIMULATION ANALYSIS

The active fault-tolerant control method for driving actuators loss of effectiveness under variable centroid conditions proposed in this paper is jointly simulated by Carsim and Matlab/Simulink to examine the control effect on the yaw stability of AGV when the control strategy takes into account both the influence of centroid change and drive loss of effectiveness. Referring to the parameters of the 4WID/4WIS AGV "Zhiyan V1" developed by the group, as shown in TABLE 3. Build the vehicle model corresponded in Carsim.

In this paper, the fault-tolerant control of single drive actuator loss of effectiveness is researched, assuming that the left front actuator fails, and the two operating conditions followed are selected for the research: the straight-line condition and the double lane change condition.

A. STRAIGHT-LINE CONDITION

The AFTC effectiveness when the single actuator of the AGV loss of effectiveness (taking the left front wheel as an example) is verified by a uniform speed straight-line

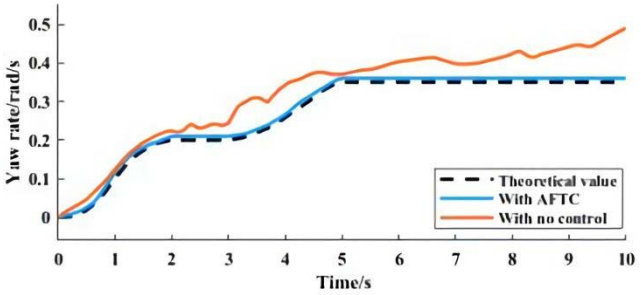

(a)Yaw rate

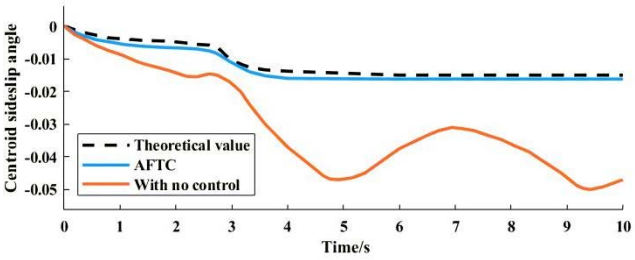

(b) Centroid sideslip angle

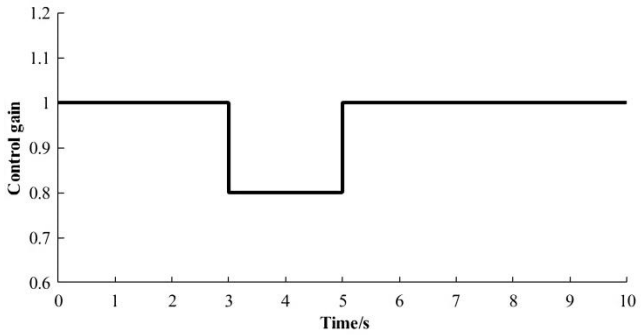

(c)Left front wheel drive actuator control gain

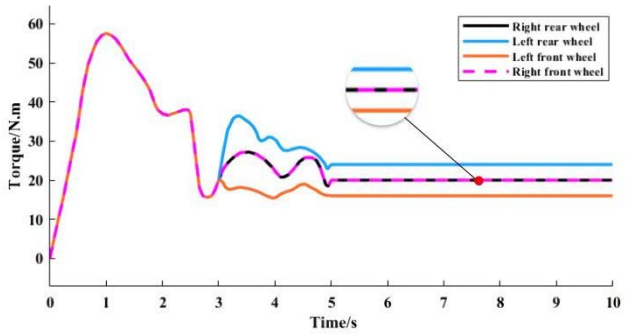

(d) Wheel torque

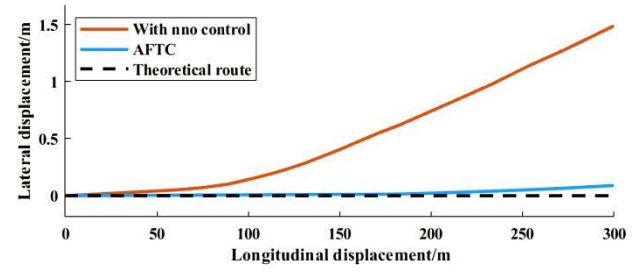

(e)motion trajectory

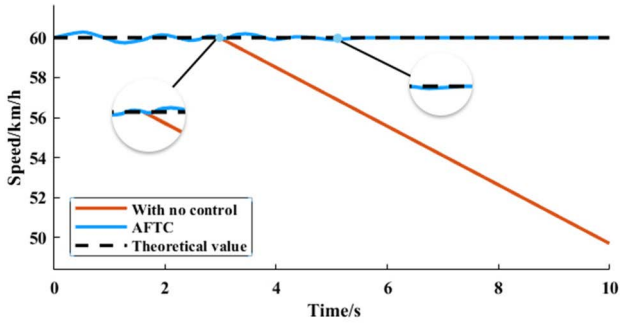

(f)Simulation speed

FIGURE 6. **Response of each parameter under straight-line conditions.**

condition. The stability of the AGV after a loss of effectiveness is determined based on parameters such as the yaw rate, the centroid sideslip angle, and the trajectory of the motion. The left front wheel drive actuator fails at t=3s. The simulation results are shown in FIGURE 6.

Refer FIGURE 6 (a) and (b), under the straight-line condition, the yaw rate and the centroid sideslip angle of the AGV should be zero. Nevertheless, according to AGV actual function, the random weight and position of cargo let the centroid position of AGV change, thus producing a certain yaw rate response and centroid sideslip angle response. At t=3s, the left front wheel drive actuator fails, causing the yaw rate response and the centroid sideslip angle response to increase, exceeding the theoretical values by 30% and 40% respectively at the peak. Comparing the three curves in the figure, it can be seen that AFTC can suppress the further expansion of the yaw rate and the centroid sideslip angle, and the error is kept within 3% from the theoretical value, which can closely follow the theoretical value. Refer FIGURE 6 (c) and (d), in the first 3s, the four-wheel torque is adjusted according to the objective function J to solve the instability caused by the change of AGV centroid position, when the left front wheel drive actuator control gains $\eta_{fl} = 1$. When t=3s, $\eta_{fl} = 0.8$, indicating that the output torque of the left front wheel drive actuator is 80% of the desired torque, the right front wheel actuator increases the torque to compensate for the lateral force, and the remaining wheel actuators adjust the torque to compensate for the longitudinal force to realize the stability of the AGV. When t=5s, the remaining wheel torque reconstruction is completed and the output torque of the left front wheel is equal to the desired torque, $\eta_{fl} = 1$. Refer FIGURE 6 (e) and (f), in the first 3s,

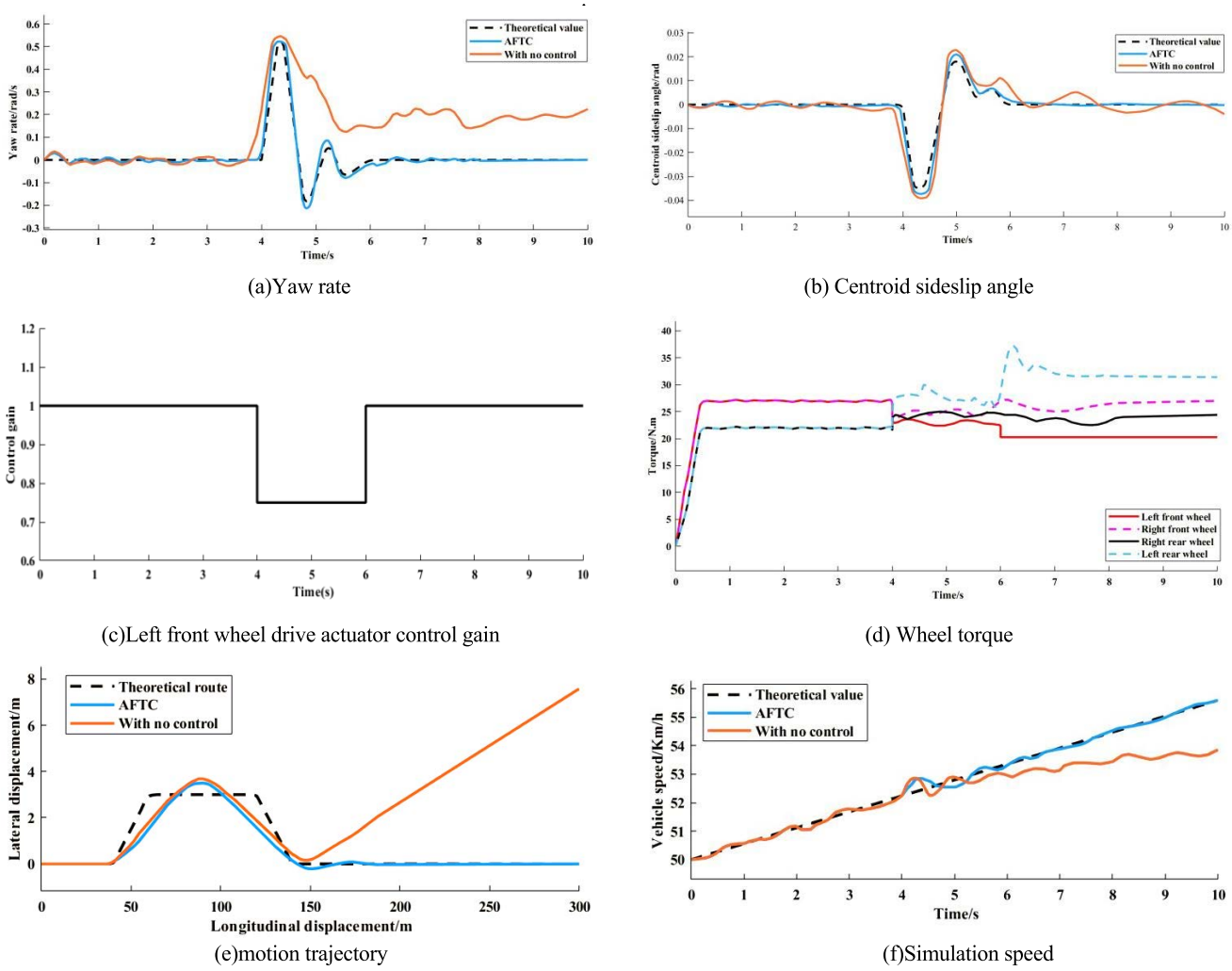

FIGURE 7. Response of each parameter under double lane change conditions.

the change of vehicle centroid position causes the AGV to slightly deviate from the straight trajectory, and the vehicle speed fluctuates around 60km/h. When the left front wheel drive actuator fails, the AFTC is able to suppress the AGV from deviating significantly from its trajectory, remaining within a 0.2m error range. The vehicle speed is able to follow the ideal vehicle speed, maintaining a constant speed of 60km/h. In the uncontrolled state, the vehicle speed drops rapidly to zero, losing kinetic energy to ensure the stability of the vehicle. In summary, under straight-line conditions,the AFTC proposed in this paper is able to achieve stability that takes into account the change of centroid position and single-wheel drive actuator loss of effectiveness.

B. DOUBLE-LINE CHANGE CONDITION

The effectiveness of AFTC when the single wheel of the AGV fails (taking the left front wheel as an example) is verified by a complex double lane change condition. The stability of the vehicle after a loss of effectiveness is determined based on wheel torque, the control gain, and simulated vehicle speed. The left front wheel drive actuator fails at t=4s. The simulation results are shown in FIGURE 7.

Refer FIGURE 7 (a) and (b), under the double lane change condition, the AGV yaw rate and centroid sideslip angle should be zero for the 0s to 4s accelerated straight-line driving part. Nevertheless, according to the actual function of AGV, the irregularity of the cargo weight and position makes the AGV centroid position change, thus producing certain yaw rate response and centroid sideslip angle response. At t=4s, the AGV changed the driving road and the left front wheel drive actuator failed, causing the yaw rate response and the centroid sideslip angle response to increase and exceed the theoretical values by 30% and 10% respectively at the peak. Comparing the three curves in FIGURE 7 (a) and (b), it can be seen that AFTC can suppress the yaw rate response and the centroid sideslip angle response, and it can follow the ideal value well, which is closer to 0 than no control. Refer FIGURE 7(c) and (d), in the first 4s, the four-wheel torque is adjusted according to the objective function J to solve the instability caused by the change of the AGV centroid position, when the left front wheel drive actuator control gains

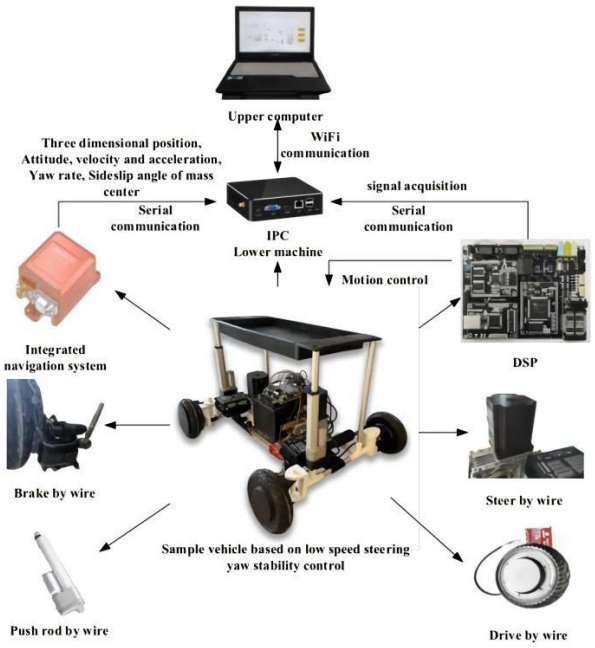

FIGURE 8. Physical picture of automated guided vehicle.

$\eta_{fl} = 1$. When t=4s, $\eta_{fl} = 0.75$, indicating that the output torque of the left front wheel drive actuator is 75% of the desired torque, the right front wheel increases to compensate the lateral force, and the other wheels adjust the torque to compensate the longitudinal force, compared with the state without control, the wheel return resistance is reduced and the stability is better controlled. When t=6s, the remaining wheel torque reconstruction is completed and the output torque of the left front wheel is equal to the desired torque, $\eta_{fl} = 1$. Refer FIGURE 7 (e) and (f), in the first 4s, the change in the vehicle's centroid position causes the AGV to deviate slightly from its straight trajectory, and the vehicle speed rises steadily from 50km/h with the double line change condition. When the left front wheel drive actuator fails, AFTC is able to suppress the AGV from deviating significantly from the trajectory, the error stays within 0.1m and the vehicle speed is able to follow the ideal vehicle speed. In the uncontrolled state, the vehicle deviates significantly from its intended trajectory. Stable control is achieved through uniform motion, and it is not possible to complete the double line change condition. In summary, the AFTC proposed in this paper can take into account the stability of centroid position change and single-wheel drive actuator loss of effectiveness under double line change condition.

V. EXPERIMENTAL VERIFICATION

A. AGV PROTOTYPE VEHICLE DESIGN

The prototype vehicle for this experiment is independently designed and manufactured 4WID/4WIS AGV, the physical expansion diagram is shown in FIGURE 8, and the vehicle parameters and motor parameters are shown in TABLE 4.

TABLE 4. Main parameters of vehicle and wheel motor.

Parameter	Value
Overall dimensions of the vehicle（long/wide/high）/*mm*	890/690/560
wheelbase /*mm*	690
Tire diameter /*mm*	200
Track width /*mm*	590
Vehicle quality /*kg*	128
Braking type	Disc electric brake
Rated output power /*W*	50-300
Rated speed /*RPM*	400
Rated torque /（*N·m*）	5
Rated voltage /*VDC*	24-48

The AGV prototype uses TMS320F28335 DSP as the lower computer for control and the embedded mini IPC as the upper computer. The four wheel motor drive actuators use a multi-method switching mode of operation to achieve optimal power and driving performance. The servo motor steering system provides closed-loop control of the heading angle of the AGV through the inertial navigation system (INS) for stable, fast and accurate operation. Linear motor let platform lifting or lowering to facilitate loading and unloading of cargoes by AGV. By extending the Kalman filter, the Aerial Head Reference System (AHRS), provides highly accurate heading, yaw and pitch angle data as well as raw data such as angular velocity and acceleration under either static or dynamic conditions. The DSP collects signals in real time and uploads them to the IPC, which issues control commands to the DSP through the CAN bus or RS232 control interface, and the DSP directly controls the corresponding equipment according to the commands. In summary, the developed AGV prototype is able to meet the experimental requirements of both straight line and double lane change conditions.

B. EXPERIMENTAL RESULTS AND ANALYSIS

Firstly, the uniform speed straight-line condition experiment is conducted. When t=3s, the DSP gives the control signal to the left front wheel drive actuator, so that the left front wheel driving actuator runs at 80% power to simulate the driving actuator fault loss of effectiveness, and the experimental results are shown in Figure 9.

Refer FIGURE 9 (a) and (b), 0s∼2s, the vehicle starts to drive after loading the cargo. The cargo placement position is irregular so that the AGV centroid position changes thus leading to fluctuations in the yaw rate and the centroid sideslip angle response. The AGV generates the instability trend or is about to be instability, but the controller does not detect the driving actuator fault loss of effectiveness. After judging by logic, nominal control of the distribution rate is adopted to distribute drive force with stability as the goal to achieve stability. From 2s to 3s, the yaw rate

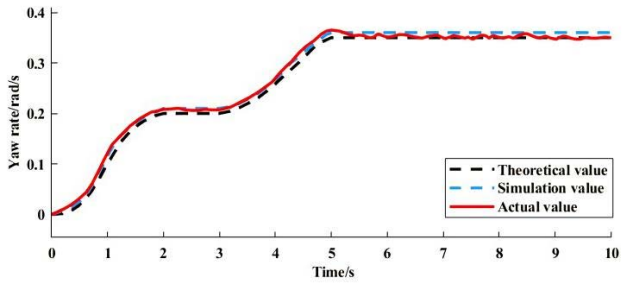

(a)Yaw rate

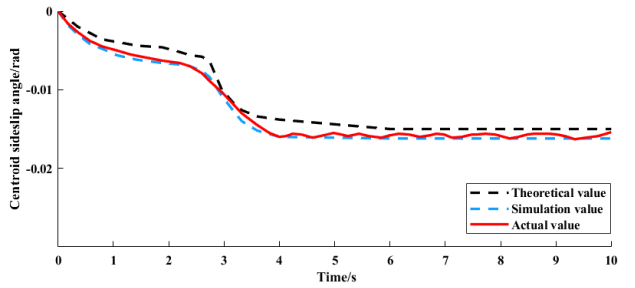

(b) Centroid sideslip angle

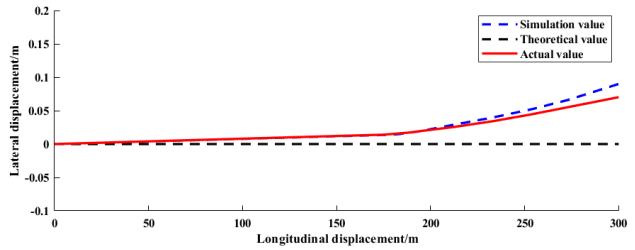

(c)motion trajectory

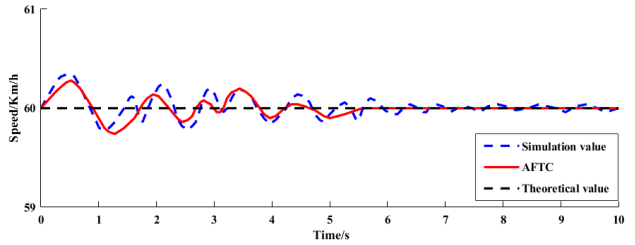

(d)Simulation speed

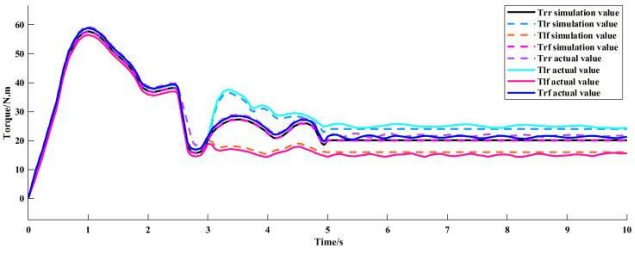

(e) Wheel torque

FIGURE 9. **Experimental parameter response under straight-line conditions.**

and the centroid sideslip response is smooth, indicating that the AGV destabilization trend is effectively controlled. At t=3s, the DSP gives a signal to the left-front driving actuator with 80% torque output to simulate a loss of effectiveness. The controller detects that the left-front control gains $\eta_{fl} = 0.8$ and immediately reconfigures the drive torque for the healthy wheel drive actuator, and the drive torque reconfiguration is completed at t=5s. After 5s, the yaw rate responce and the centroid sideslip angle responce gradually stabilized, indicating that the AGV was in a stable state. Refer FIGURE 9 (c), AFTC can well suppress the degree of trajectory deviation after the driving actuator loss of effectiveness and ensure the safety of driving. Refer FIGURE 9 (d), the change of the centroid position and the driving actuator loss of effectiveness produces fluctuations in the vehicle speed, and the actual speed can still closely follow the theoretical value under the AFTC action. Refer FIGURE 9(e), the variation of the output torque of each drive actuator is seen more visually. Instability due to change in the centroid position, uniform distribution of driving torque among wheels in the absence of the driving actuator loss of effectiveness. After 3s, the left-front driving actuator fails and the driving torque decreases. The healthy wheels remained carry out drive reconfiguration to generate additional yaw moment to compensate for the vehicle yaw moment around the centroid to achieve AGV stability. In summary, under straight-line conditions,the AFTC proposed in this paper is able to achieve stability that takes into account the change of centroid position and single-wheel driving actuator loss of effectiveness.

Next, a double lane change condition experiment was conducted.When t=4s, the DSP gave the control signal to the left front wheel drive actuator to make the left front wheel drive actuator run at 75% power to simulate the driving actuator loss of effectiveness, and the experimental results are shown in FIGURE 10.

Refer FIGURE 10 (a) and (b), the position of the centroid changes after the AGV is loaded with cargo during 0s∼4s. The fluctuations in the yaw rate and the centroid sideslip angle indicate that the AGV has a tendency to be unstable or is about to be unstable. At this time, the control gain of each wheel drive actuator is 1. The nominal control distribution rate is adopted, and the driving force is distributed with stability as the goal to realize the stability of AGV. At t=4s, the DSP gives the signal to the left front wheel drive actuator, the left-front actuator control gains $\eta_{fl} = 0.8$, and the controller immediately reconstructs the drive torque for the rest of the wheel drive actuator. t=6s, the drive torque reconstruction is completed. After t=6s, the yaw rate and the centroid sideslip angle response is gradually stabilized, indicating that the AGV is in a stable state. Refer FIGURE 10(c), AFTC is able to closely follow the predetermined driving trajectory to ensure the safety of driving. Refer FIGURE 10(d), the change of the centroid position and the drive actuator loss of effectiveness produced fluctuations on the vehicle speed, and the actual speed was able to remain stable under the AFTC action. Refer FIGURE 10(e), the variation of the output torque of each drive actuator is seen more visually. Instability due to change in the centroid position, uniform distribution of drive torque

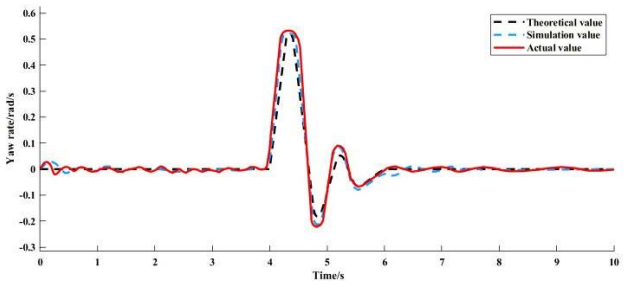

(a)Yaw rate

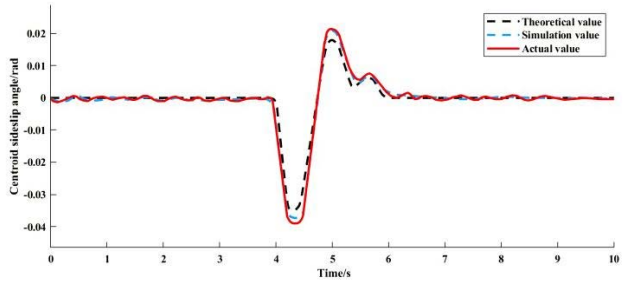

(b) Centroid sideslip angle

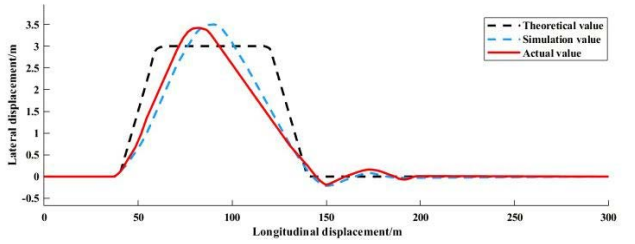

(c)motion trajectory

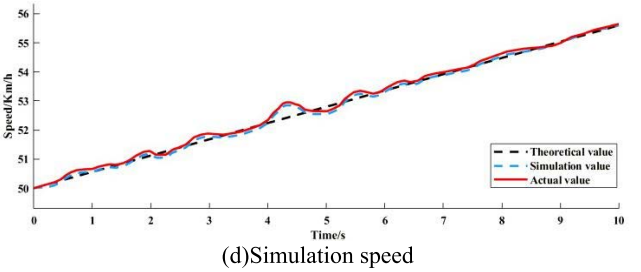

(d)Simulation speed

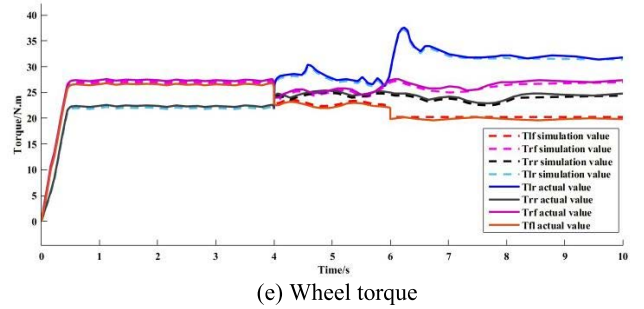

(e) Wheel torque

FIGURE 10. **Experimental parameter response under double lane change conditions.**

among wheels in the absence of drive actuator loss of effectiveness. After 4s, the left front drive actuator fails and the drive torque decreases. The healthy actuator remained carry out drive reconfiguration to generate additional yaw moment to compensate for the vehicle yaw moment around the centroid to achieve AGV stability control. In summary, the AFTC proposed in this paper can take into account the stability of centroid position change and single-wheel drive actuator loss of effectiveness under double lane change condition.

VI. CONCLUSION

1) In this paper, the 4WID/4WIS AGV is used as the research object. The three-degree-of-freedom model of the vehicle body, the driving-wheel model, the HSRI tire model and the actuator loss of effectiveness model established to provide a theoretical basis for modeling in Simulink.

2) A hierarchical AFTC strategy is designed to address the problem of the driving actuator loss of effectiveness affecting the completion of handling tasks under AGV variable centroid conditions. The upper layer is an MPC-based optimal input solver controller, which solves the optimal state input of the AGV and establishes the 2-DOF ideal model. The middle layer is a fuzzy theory based expectation target moment solver, which solves the ideal additional yaw moment and establishes the driving torque distribution method based on the objective stability function. The lower layer is a control gain based driving torque reconfiguration distribution controller, which reconfigures the driving moments remained of the healthy wheels to ensure the stability of the AGV when the position of the centroid changes and the single-wheel driving actuator fails.

3) A joint simulation platform based on Carsim and Matlab/Simulink was established for testing. The vehicle model and simulation conditions are established in Carsim environment, and the driving wheel model, the actuator loss of effectiveness model and the controller model established in Simulink. After adding AFTC control, the yaw rate and centroid sideslip angle can closely track the theoretical values and keep the error within 4%. The travel trajectory and vehicle speed simulated is corrected and kept stable. The simulation results show the reasonableness of the established AFTC strategy under straight line and double lane change conditions, which can improve the stability of AGV under the change of centroid position and single-wheel drive actuator loss of effectiveness.

4) Real-vehicle experiments on the control strategy were conducted, and a 4WID/4WIS AGV prototype was developed to simulate the handling task between two workstations in a straight-line scenario and a double lane change scenario in a factory. The experiments show that the yaw rate and centroid sideslip angle is within 5% of the theoretical value, and there is no significant change in driving trajectory and vehicle speed. The ATFC control strategy designed in this paper can reduce the delay, accelerate the response speed and improve the stability of the AGV. The experimental results are basically consistent with the simulation results, which verifies the correctness of the algorithm.

ACKNOWLEDGMENT

The authors would like to thank Dr. Ni for assistance with the experiments and to Dr. Zhao for valuable discussion.

REFERENCES

[1] S. Liu, J. Yu, X. Deng, and S. Wan, "FedCPF: An efficient-communication federated learning approach for vehicular edge computing in 6G communication networks," *IEEE Trans. Intell. Transp. Syst.*, vol. 23, no. 2, pp. 1616–1629, Feb. 2022, doi: 10.1109/TITS.2021.3099368.

[2] S. Zhu, Q. Fu, X. Huang, Z. Wang, and X. Yang, "Motor fault diagnosis and failure control for distributed four-wheel drive electric vehicles," *Automot. Eng.*, vol. 42, no. 9, pp. 1284–1291, Oct. 2020, doi: 10.19562/j.Chinasae.qcgc.2020.09.020.

[3] W. B. Chu, "Rule-based traction system failure control of distributed electric drive vehicle," *J. Mech. Eng.*, vol. 48, no. 10, pp. 90–95 and 102, May 2012, doi: 10.3901/JME.2012.10.090.

[4] W. Liu, Y. Yu, Q. Zhang, Y. Wan, and M. Wang, "Optimal torque distribution of distributed driving AGV under the condition of centroid change," *Sci. Rep.*, vol. 11, no. 1, 2021, Art. no. 21404, doi: 10.1038/s41598-021-01038-3.

[5] B. Zhang and S. Lu, "Fault-tolerant control for four-wheel independent actuated electric vehicle using feedback linearization and cooperative game theory," *Control Eng. Pract.*, vol. 101, Jun. 2020, Art. no. 104510, doi: 10.1016/j.conengprac.2020.104510.

[6] B. Zhang, S. Lu, W. Wu, C. Li, and J. Lu, "Robust fault-tolerant control for four-wheel individually actuated electric vehicle considering driver steering characteristics," *J. Franklin Inst.*, vol. 358, no. 11, pp. 5883–5908, May 2021, doi: 10.1016/j.jfranklin.2021.05.034.

[7] Y.-D. Song, H.-N. Chen, and D.-Y. Li, "Virtual-point-based fault-tolerant lateral and longitudinal control of 4W-steering vehicles," *IEEE Trans. Intell. Transp. Syst.*, vol. 12, no. 4, pp. 1343–1351, Dec. 2011, doi: 10.1109/TITS.2011.2158646.

[8] D. Zhang, G. Liu, H. Zhou, and W. Zhao, "Adaptive sliding mode fault-tolerant coordination control for four-wheel independently driven electric vehicles," *IEEE Trans. Ind. Electron.*, vol. 65, no. 11, pp. 9090–9100, Nov. 2018, doi: 10.1109/TIE.2018.2798571.

[9] J. He, L. Mi, S. Mao, C. Zhang, and H. Chu, "Fault-tolerant control of a nonlinear system actuator fault based on sliding mode control," *J. Control Sci. Eng.*, vol. 2017, pp. 1–13, Mar. 2017, doi: 10.1155/2017/8595960.

[10] B. Guo and Y. Chen, "Robust adaptive fault-tolerant control of four-wheel independently actuated electric vehicles," *IEEE Trans. Ind. Informat.*, vol. 16, no. 5, pp. 2882–2894, May 2020, doi: 10.1109/TII.2018.2889292.

[11] T. Chen, L. Chen, X. Xu, Y. Cai, H. Jiang, and X. Sun, "Passive fault-tolerant path following control of autonomous distributed drive electric vehicle considering steering system fault," *Mech. Syst. Signal Process.*, vol. 123, pp. 298–315, Jan. 2019, doi: 10.1016/j.ymssp.2019.01.019.

[12] B. Li, H. Du, and W. Li, "Fault-tolerant control of electric vehicles with in-wheel motors using actuator-grouping sliding mode controllers," *Mech. Syst. Signal Process.*, vols. 72–73, pp. 462–485, Dec. 2015, doi: 10.1016/j.ymssp.2015.11.020.

[13] J. Liu, C. Liu, C.-F. Zong, and H. Zheng, "Fault-tolerant control of 4WID/WIS electric vehicles based on reconfigurable control allocation," *J. South China Univ. Technol. Natural Sci. Edition*, vol. 41, no. 11, pp. 125–131, Apr. 2013, doi: 10.3969/j.issn.1000-565X.2013.11.021.

[14] R. Wang and J. Wang, "Fault-tolerant control with active fault diagnosis for four-wheel independently driven electric ground vehicles," *IEEE Trans. Veh. Technol.*, vol. 60, no. 9, pp. 4276–4287, Nov. 2011, doi: 10.1109/TVT.2011.2172822.

[15] L. Zhang, Y. Wen, Z. Wang, and X. Ding, "Fault tolerant control based on multi-methods switching four-wheel-independently-actuated electric vehicle," *J. Mech. Eng.*, vol. 56, no. 16, pp. 227–239, Aug. 2020, doi: 10.3901/JME.2020.16.227.

[16] A. Mihály, P. Gáspár, and B. Németh, "Multiple fault-tolerant in-wheel vehicle control based on high-level control reconfiguration," *IFAC-PapersOnLine*, vol. 50, no. 1, pp. 8606–8611, Aug. 2017, doi: 10.1016/j.ifacol.2017.08.1428.

[17] L. J. Liu, K. Shi, and X. F. Yuan, "Multiple model-based fault-tolerant control system for distributed drive electric vehicle," *J. Braz. Soc. Mech. Sci. Eng.*, vol. 41, p. 531, Nov. 2019, doi: 10.1007/s40430-019-2047-6.

[18] A. Imane, M. N. Kabbaj, and M. Benbrahim, "Fault tolerant control of vehicle lateral dynamic using a new pneumatic forces multiple model," *Actuators*, vol. 9, no. 4, p. 120, Nov. 2020, doi: 10.3390/ACT9040120.

[19] P. Li, P. Li, J. Zhao, and B. Zhang, "Non-fragile multi-objective linear parameter-varying controller design for vehicle lateral stability," *IET Control Theory Appl.*, vol. 14, no. 18, pp. 2717–2725, Oct. 2020, doi: 10.1049/iet-cta.2020.0514.

[20] A. Lopes and R. E. Araujo, "Fault-tolerant control based on sliding mode for overactuated electric vehicles," in *Proc. IEEE Int. Electr. Vehicle Conf. (IEVC)*, Dec. 2014, pp. 1–6, doi: 10.1109/IEVC.2014.7056137.

[21] J. S. Im, F. Ozaki, T. K. Yeu, and S. Kawaji, "Model-based fault detection and isolation in steer-by-wire vehicle using sliding mode observer," *J. Mech. Sci. Technol.*, vol. 23, no. 8, pp. 1991–1999, 2009, doi: 10.1007/s12206-009-0357-9.

[22] Y. G. Luo, R. Chen, and Y. Hu, "Active fault-tolerant control based on MFAC or 4WID EV with steering by wire system," *J. Mech. Eng.*, vol. 55, no. 22, pp. 131–139, Nov. 2019, doi: 10.3901/JME.2019.22.131.

[23] Y. Hu, J. Fachao, C. Rui, and L. Yugong, "Active fault-tolerant control based on MFAC for 4WID EV driving system," *Automot. Eng.*, vol. 41, no. 9, pp. 983–989 and 1005, Nov. 2019, doi: 10.19562/j.Chinasae.qcgc.2019.09.001.

[24] Y. Luo, Y. Hu, F. Jiang, R. Chen, and Y. Wang, "Active fault-tolerant control based on multiple input multiple output-model free adaptive control for four wheel independently driven electric vehicle drive system," *Appl. Sci.*, vol. 9, no. 2, p. 276, Jan. 2019, doi: 10.3390/app9020276.

[25] X. Liu, Y.-W. Wang, D. Chen, and H. Chen, "Adaptive fuzzy fault-tolerant control for a class of unknown non-linear dynamical systems," *IET Control Theory Appl.*, vol. 10, no. 18, pp. 2357–2369, Dec. 2016, doi: 10.1049/iet-cta.2016.0826.

[26] Y. Luo, J. Luo, and Z. Qin, "Model-independent self-tuning fault-tolerant control method for 4WID EV," *Int. J. Automot. Technol.*, vol. 17, no. 6, pp. 1091–1100, Dec. 2016, doi: 10.1007/s12239-016-0106-x.

[27] W. T. Wei, R. Yang, H. Gu, W. Zhao, C. Chen, and S. Wan, "Multi-objective optimization for resource allocation in vehicular cloud computing networks," *IEEE Trans. Intell. Transp. Syst.*, early access, Aug. 3, 2021, doi: 10.1109/TITS.2021.3091321.

[28] C. Chen, Y. Zhang, Z. Wang, S. Wan, and Q. Pei, "Distributed computation offloading method based on deep reinforcement learning in ICV," *Appl. Soft Comput.*, vol. 103, May 2021, Art. no. 107108, doi: 10.1016/j.asoc.2021.107108.

[29] Y. Wang, J. Gao, K. Li, and H. Chen, "Integrated design of control allocation and triple-step control for over-actuated electric ground vehicles with actuator faults," *J. Franklin Inst.*, vol. 357, no. 6, pp. 3150–3167, Sep. 2019, doi: 10.1016/j.jfranklin.2019.07.035.

[30] N. Wada, K. Fujii, and M. Saeki, "Reconfigurable fault-tolerant controller synthesis for a steer-by-wire vehicle using independently driven wheels," *Vehicle Syst. Dyn.*, vol. 51, no. 9, pp. 1438–1465, Aug. 2013, doi: 10.1080/00423114.2013.806671.

[31] G. Zhang, H. Zhang, X. Huang, J. Wang, H. Yu, and R. Graaf, "Active fault-tolerant control for electric vehicles with independently driven rear in-wheel motors against certain actuator faults," *IEEE Trans. Control Syst. Technol.*, vol. 24, no. 5, pp. 1557–1572, Nov. 2015, doi: 10.1109/TCST.2015.2501354.

[32] Y. Yu and Y. Dong, "Global fault-tolerant control of underactuated aerial vehicles with redundant actuators," *Int. J. Aerosp. Eng.*, vol. 2019, pp. 1–12, Feb. 2019, doi: 10.1155/2019/9754981.

[33] X. Z. Jin, Y. G. He, and Y. G. He, "Finite-time robust fault-tolerant control against actuator faults and saturations," *IET Control Theory Appl.*, vol. 11, pp. 550–556, Dec. 2016, doi: 10.1049/iet-cta.2016.1144.

[34] T. H. Nguyen, B.-C. Chen, D. Yin, and P.-S. Huynh, "Active fault tolerant torque distribution control of 4 in-wheel motors electric vehicles based on Kalman filter approach," in *Proc. Int. Conf. Syst. Sci. Eng. (ICSSE)*, 2017, pp. 360–364, doi: 10.1109/ICSSE.2017.8030897.

[35] H. Zhou, F. Jia, Z. Liu, and H. Liu, "Fault diagnosis and fault-tolerant control method for in-wheel motor electric vehicles," *J. Mech. Eng.*, vol. 55, no. 22, pp. 174–182, Nov. 2019, doi: 10.3901/JME.2019.22.174.

[36] Y. Liu, C. Zong, D. Zhang, H. Zheng, X. Han, and M. Sun, "Fault-tolerant control approach based on constraint control allocation for 4WIS/4WID vehicles," *Proc. Inst. Mech. Eng., D, J. Automobile Eng.*, vol. 235, no. 8, pp. 2281–2295, Jul. 2021, doi: 10.1177/0954407020982838.

[37] M. Naderi, T. A. Johansen, and A. K. Sedigh, "A fault tolerant control scheme using the feasible constrained control allocation strategy," *Int. J. Autom. Comput.*, vol. 16, no. 5, pp. 628–643, Oct. 2019, doi: 10.1007/s11633-019-1168-9.

[38] A. Mbarek and K. Bouzrara, "Fault tolerant control for MIMO nonlinear systems via MPC based on MIMO ARX-Laguerre multiple models," *Math. Problems Eng.*, vol. 2019, p. 26, Oct. 2019, doi: 10.1155/2019/9012182.

[39] M. M. Tavakoli and N. Assadian, "Actuator failure-tolerant control of an all-thruster satellite in coupled translational and rotational motion using neural networks," *Int. J. Adapt. Control Signal Process.*, vol. 32, no. 12, pp. 1748–1763, Dec. 2018, doi: 10.1002/acs.2942.

[40] A. Kiselev, G. R. Catuogno, A. Kuznietsov, and R. Leidhold, "Finite-control-set MPC for open-phase fault-tolerant control of PM synchronous motor drives," *IEEE Trans. Ind. Electron.*, vol. 67, no. 6, pp. 4444–4452, Jun. 2020, doi: 10.1109/TIE.2019.2931285.

[41] W. Liu, Q. Zhang, Y. Wan, P. Liu, Y. Yu, and J. Guo, "Yaw stability control of automated guided vehicle under the condition of centroid variation," *J. Brazilian Soc. Mech. Sci. Eng.*, vol. 44, no. 1, pp. 1–5, Jan. 2022, doi: 10.1007/S40430-021-03321-W.

[42] C. Huang, F. Naghdy, and H. Du, "Delta operator-based fault estimation and fault-tolerant model predictive control for steer-by-wire systems," *IEEE Trans. Control Syst. Technol.*, vol. 26, no. 5, pp. 1810–1817, Aug. 2017, doi: 10.1109/TCST.2017.2736497.

[43] Y. Wang, C. Zong, K. Li, and H. Chen, "Fault-tolerant control for in-wheel-motor-driven electric ground vehicles in discrete time," *Mech. Syst. Signal Process.*, vol. 121, pp. 441–454, Nov. 2018, doi: 10.1016/j.ymssp.2018.11.030.

[44] J. Zhao, Y. Lu, B. Zhu, and S. Liu, "Estimation algorithm for longitudinal and vertical forces of smart tire with accelerometer embedded," *Automot. Eng.*, vol. 40, no. 2, pp. 137–183, Sep. 2018, doi: 10.19562/j.Chinasae.Qcgc.2018.02.003.

QINGJIE ZHANG was born in Jiangsu, China, in 1998. He is currently pursuing the master's degree in mechanical engineering with the School of Automotive Engineering, Yancheng Institute of Technology, China. His research interest includes vehicle stability control.

WEI LIU was born in Jiangsu, China, in 1986. He received the B.S. and Ph.D. degrees from the Nanjing University of Science and Technology, China, in 2012. He is currently working as an Associate Professor with the School of Automotive Engineering, Yancheng Institute of Technology, China. His research interests include intelligent system design and vehicle dynamics control.

PING LIU was born in Shanxi, China, in 1997. She is currently pursuing the master's degree in mechanical engineering with the School of Automotive Engineering, Yancheng Institute of Technology, China. Her research interests include vehicle power and economy.